ELSEVIER

Journal of Alloys and Compounds 446–447 (2007) 178–182

Journal of ALLOYS AND COMPOUNDS

www.elsevier.com/locate/jallcom

The effect of solidification rate on microstructural evolution of a melt-spun Mg–20Ni–8Mm hydrogen storage alloy

Ying Wu [a,*], Jan Ketil Solberg [a], Volodymyr A Yartys [a,b]

[a] *Department of Materials Technology, Norwegian University of Science and Technology, NO-7491 Trondheim, Norway*
[b] *Institute for Energy Technology, P.O. Box 40, N-2027 Kjeller, Norway*

Received 27 October 2006; received in revised form 23 November 2006; accepted 1 December 2006
Available online 16 January 2007

Abstract

Mg-based Mg–20Ni–8Mm (wt%) (Mm = Ce, La-rich Mischmetal) hydrogen storage alloy with microcrystalline, nanocrystalline, and amorphous microstructures was obtained by controlling the solidification rate of the melt-spun ribbon. The microstructure was remarkably refined by rapid solidification compared with that of a conventionally prepared polycrystalline alloy. The optimal microstructure with a considerable amount of nanocrystalline Mg and Mg_2Ni in an amorphous matrix was expected to have the highest hydrogen storage capacity. Mischmetal-containing $Mg_{12}Mm$ intermetallic precipitated preferentially at the boundary of magnesium grains in the microcrystalline microstructure, thus providing possible pathways for the enhanced hydrogen diffusion into the Mg.

Keywords: Hydrogen absorbing materials; Rapid-solidification; Microstructure; Transmission electron microscopy

1. Introduction

Mg-based alloys have been considered as very promising candidates for hydrogen storage systems due to their low specific weight, high hydrogen storage capacity, and rich natural resources. However, high hydrogen desorption temperature (300 °C) and relatively slow kinetics of H-absorption/desorption make them still far from being practically applicable. In order to improve the hydrogen storage applicability of the Mg-based alloys, several methods such as adding transition metals and rare-earth elements have been employed to modify the reaction thermodynamics and to enhance H-sorption kinetics. Mechanical alloying [1–9] and rapid solidification [10–19] methods have been applied to produce nanosize level grains and even amorphous microstructures to improve the hydrogenation characteristics. The mechanical alloying process generally involves the reduction of grain size and the formation of various defects, which shorten the diffusion length of hydrogen and increase the number of active sites for hydrogenation.

Unlike traditional alloys, several factors such as chemical composition, processing, and microstructure, particularly grain size, have effect on the hydrogen storage capacity as well as the kinetics of hydrogen absorption of the Mg-based alloys. Compared with the conventional crystalline Mg-based alloys, nanocrystalline alloys as well as alloys containing nanocrystalline and amorphous phases exhibit much faster kinetics of H-absorption/desorption and lower temperature of hydriding/dehydriding. The large number of interfaces and grain boundaries available in the nanocrystalline materials provide easy pathways for hydrogen diffusion and promote the absorption of hydrogen [11]. Nanocrystalline Mg_2Ni-based alloys are known to exhibit higher H-absorption capacities and faster kinetics of hydriding/dehydriding than crystalline Mg_2Ni [10,17]. Therefore, a suitable microstructure is one of the keys to obtain optimized hydrogen storage properties.

In the present study, microcrystalline, nanocrystalline, and amorphous Mg–20Ni–8Mm alloys were prepared by rapid solidification, and the microstructure evolution under various cooling rates in the melt-spun ribbons was studied and compared with the as-cast master alloy focusing on obtaining a stable microstructure for large hydrogen absorption capacity.

2. Experimental

The master alloy was prepared by induction melting of a mixture of 99.7% pure cerium and lanthanum rich Mischmetal, 99.98% pure magnesium and

* Corresponding author. Tel.: +47 7359 5164; fax: +47 7355 0203.
E-mail address: ying.wu@material.ntnu.no (Y. Wu).

0925-8388/$ – see front matter © 2006 Elsevier B.V. All rights reserved.
doi:10.1016/j.jallcom.2006.12.002

99.98% pure nickel. The melting was performed in a vacuum furnace under an argon atmosphere. The melt-spun ribbons were obtained by a single roller melt-spinning technique (copper quenching disc with a diameter of 200 mm) in an argon atmosphere of 200 mbar. The surface velocity of the wheel was adjusted in three steps from 3.1, 10.5 to 20.9 ms^{-1}. The structure, composition, and morphology of the phases were examined by X-ray diffractometry (XRD), scanning electron microscopy (SEM, Hitachi s-4300se), and transmission electron microscopy (TEM, JEM-2010) equipped with an energy-dispersive X-ray spectrometry (EDS).

3. Results

3.1. Phase composition and structure of the master alloy

The as-cast master alloy has a typical dendritic microstructure. As shown in Fig. 1, the microstructures consisted of mainly Mg_2Ni with a size of 2–80 μm and a minor Mischmetal-containing Mg-rich phase in a matrix of Mg. By combining the results of EDS and XRD, the Mischmetal-containing phases were determined to be $Mg_{12}Mm$ and $Mg_{17}Mm_2$ (bright contrast in the micrograph).

3.2. Microstructure and morphology of melt-spun alloy

Fig. 2 shows XRD diffraction spectra of melt-spun Mg–20Ni–8Mm alloy with different solidification rates. When the surface velocity of the copper wheel was 20.9 ms^{-1}, the highest solidification rate of the melt-spun was obtained, resulting in the lower intensities of the XRD spectrum (Fig. 2(a)). Two broad peaks from amorphous phase constituents appeared in the diffraction pattern with maximums at 18 and 37.5° for melt-spun ribbon. In addition, crystallization of Mg_2Ni and, to a lesser extent, Mg was evident. A TEM image and its corresponding selected area diffraction pattern (SADP) are shown in Fig. 3(a). Only featureless contrast over the entire bright field image and halo rings with no spotty diffraction patterns were clearly observable. However, weak diffraction peaks from crystalline phases of Mg and Mg_2Ni were occasionally observed,

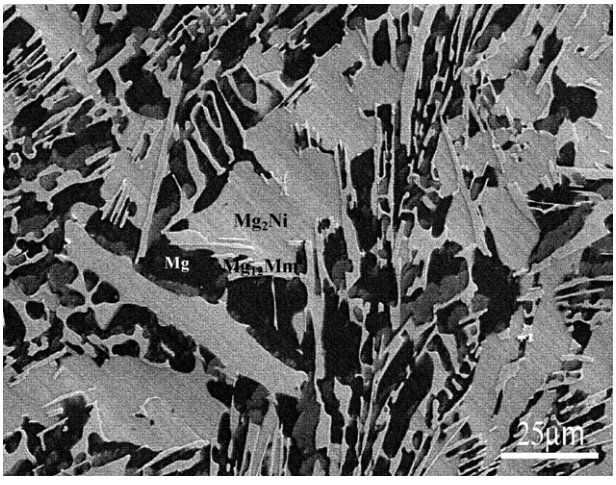

Fig. 1. SEM micrograph showing the typical dendritic microstructure of the as-cast Mg–20Ni–8Mm alloy. The microstructure consists of mainly Mg_2Ni (gray areas) and a minor Mischmetal-rich Mg-containing phase (bright areas, $Mg_{12}Mm$ and $Mg_{17}Mm_2$) in a matrix of Mg (dark areas).

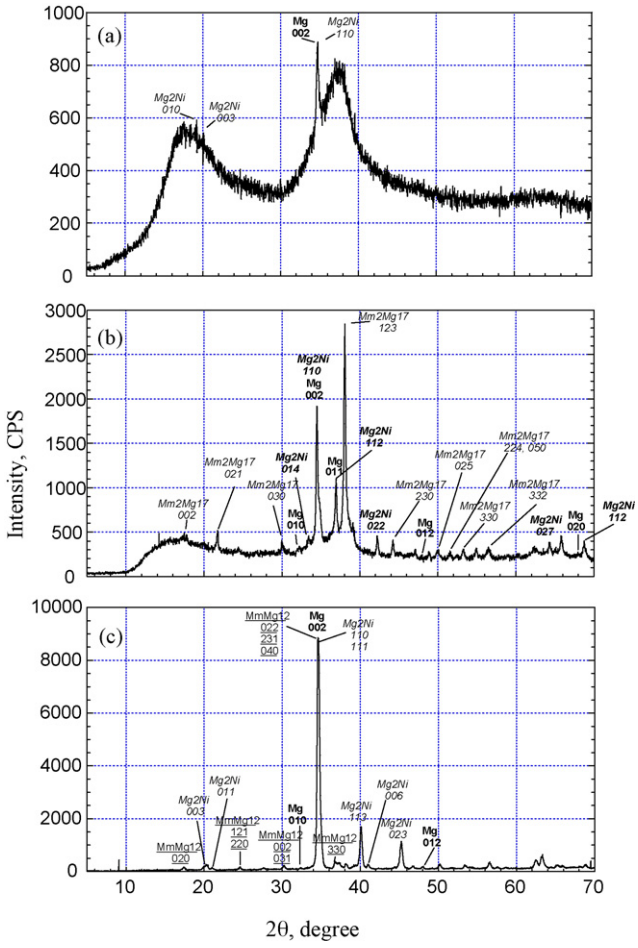

Fig. 2. XRD diagrams of melt-spun Mg–20Ni–8Mm solidified at different surface velocities of the copper wheel: (a) 20.9, (b) 10.5, and (c) 3.1 ms^{-1}. The refinements of the data yielded the following values of the unit cell parameters; Mg: space group $P6_3/mmc$; $a = 3.193(1)$; $c = 5.195(2)$ Å; Mg_2Ni: space group $P6_222$; $a = 5.20(1)$; $c = 13.21(4)$ Å; $Mg_{12}Ce$: space group $I4/mmm$; $a = 10.31(3)$; $c = 5.90(3)$ Å; $Mg_{17}La_2$: space group $P6_3/mmc$; $a = 10.307(7)$; $c = 9.96(1)$ Å.

resulting in small peaks in the XRD spectrum (Fig. 2). As shown in Fig. 3(b), a minor amount of nanocrystalline equiaxed Mg grains and rod-shaped Mg_2Ni particles are formed in the amorphous matrix. Thus, the melt-spun ribbon was mainly composed of an amorphous single phase except for a minor amount of nanocrystalline Mg and Mg_2Ni particles.

The amount of nanocrystalline phases significantly increased when decreasing the surface velocity of the copper wheel to 10.5 ms^{-1}. As shown in Fig. 2(b), strong diffraction peaks of Mg and Mg_2Ni phases appeared in the specimen for this intermediate solidification rate, and $Mg_{17}Mm_2$ was formed instead of $Mg_{12}Mm$. Fig. 4 shows typical TEM micrographs of the microstructures of this melt-spun ribbon. In accordance with the result of XRD, a small amount of amorphous matrix remained in the specimen as shown in Fig. 4(a), in addition to nanocrystalline equiaxed Mg particles of about 10 nm size, giving the inserted [1 0 1] zone axis SADP. However, most of the matrix in the specimen was in the crystalline state, see Fig. 4(b), which shows a considerable amount of intermixed nanocrystalline particles of Mg and Mg_2Ni indicated by the inserted SADP. The enlarged

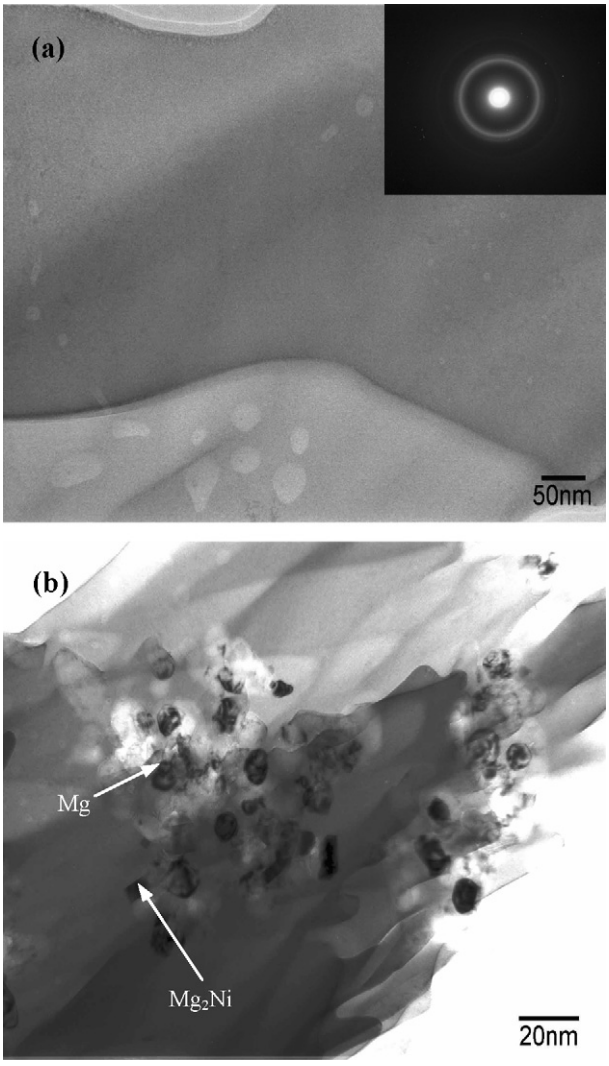

Fig. 3. TEM micrographs showing the microstructures of melt-spun Mg–20Ni–8Mm alloy at a surface velocity of the copper wheel of 20.9 ms^{-1}: (a) amorphous matrix and its corresponding SADP, (b) nanocrystalline phases of Mg and Mg_2Ni particles.

micrograph in Fig. 4(c) shows further details of the microstructure containing nanocrystalline Mg and Mg_2Ni particles in an amorphous matrix. Thus, the microstructure was composed of a large amount of nanocrystalline phases of Mg and Mg_2Ni particles and a minor amount of amorphous phase as well as a slight amount of Mischmetal-rich phases.

When the surface velocity of the copper wheel was 3.1 ms^{-1}, the lowest solidification rate was obtained, and the melt-spun specimen was fully crystalline. Three phases, that is Mg, Mg_2Ni, and $Mg_{12}Mm$ phases, can be identified in Fig. 2(c). The two former phases, Mg and Mg_2Ni, because of their significantly higher content in the material, are represented by the strongest peaks in the diffraction pattern compared to rather weak peaks associated with the minority phase in the alloy, $Mg_{12}Mm$ intermetallic. Figs. 5(a)–(d) show TEM micrographs of the ribbon that was melt-spun at the lowest solidification rate. As shown in Fig. 5(a), two types, that is rod-shaped and equiaxed grains, were observed. EDS and SADP analysis identified the rod-shaped

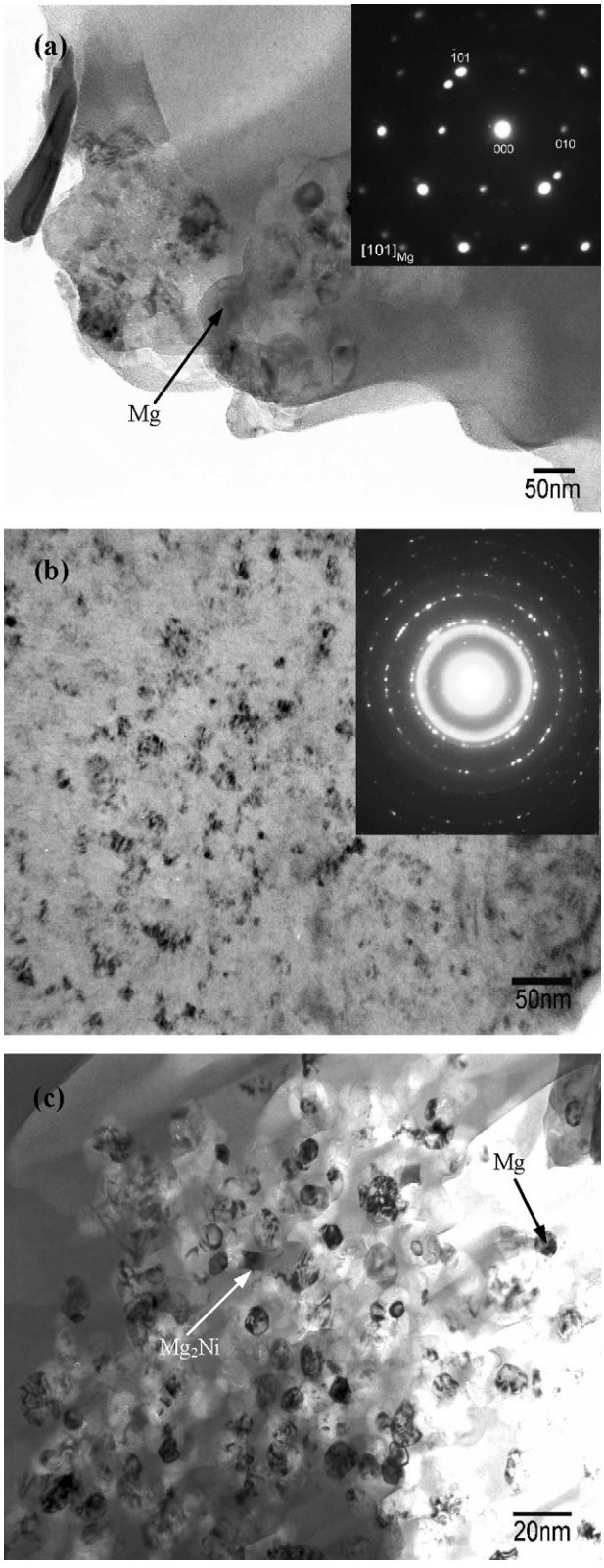

Fig. 4. TEM micrographs with corresponding SADPs showing the microstructures of melt-spun Mg–20Ni–8Mm applying a surface velocity of the copper wheel of 10.5 ms^{-1}: (a) amorphous matrix, (b) nanocrystalline mixture of Mg matrix and Mg_2Ni particles, and (c) nanocrystalline phases of Mg and Mg_2Ni particles in an amorphous matrix (detail from (b)).

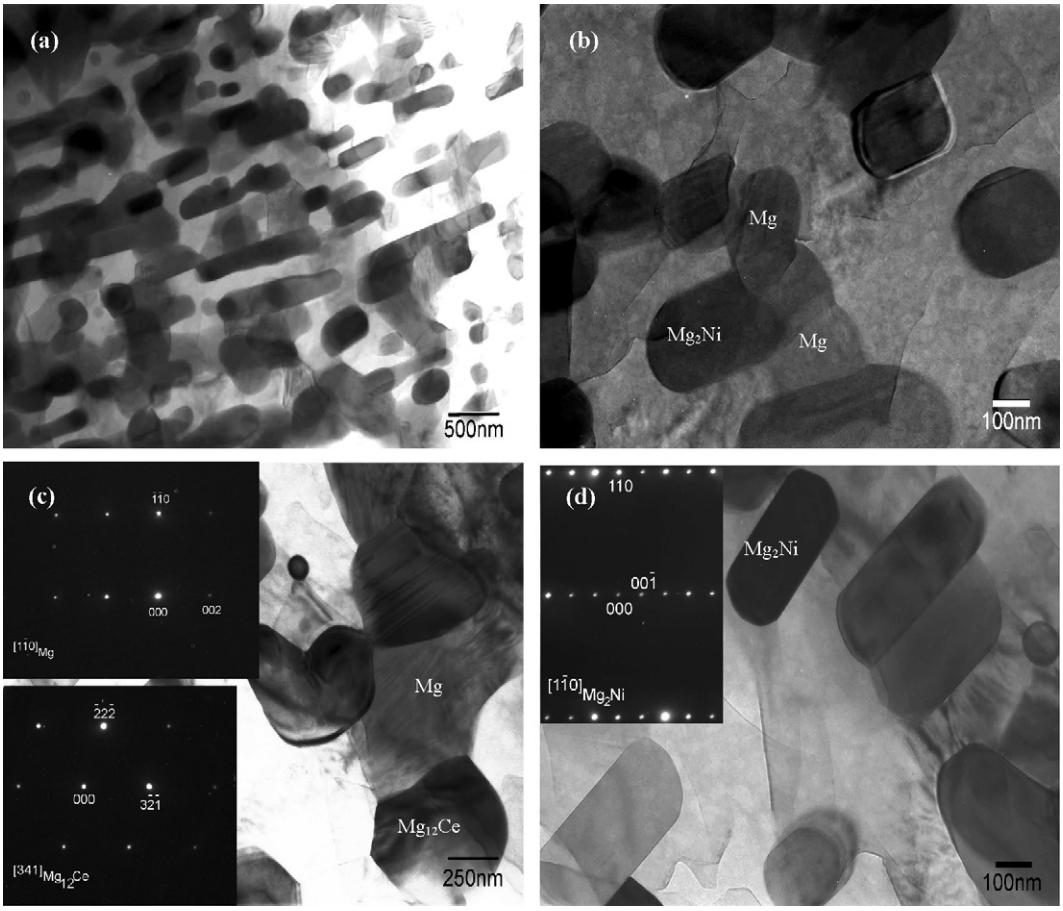

Fig. 5. TEM micrographs showing the microstructures of melt-spun Mg–20Ni–8Mm produced with a surface velocity of the copper wheel of 3.1 ms^{-1}: (a) overall morphology, (b) high magnification image of Mg_2Ni and Mg particles, (c) microcrystalline Mg and $Mg_{12}Ce$ with their respective [1 $\bar{1}$ 0] and [3 4 1] zone axis SADPs, and (d) microcrystalline Mg_2Ni and its [1 $\bar{1}$ 0] zone axis SADP.

grains as Mg_2Ni, the equiaxed grains were determined to be Mg and Mischmetal-rich particles. From the high magnification micrograph of Fig. 5(b), the average size of equiaxed Mg particles is determined to be 0.4 μm. Fig. 5(c) shows a typical $Mg_{12}Ce$ particle with a coarse size of approximately 0.8 μm and its corresponding [3 4 1] zone axis SADP. It is clear that the $Mg_{12}Ce$ particles preferred to locate at the boundary of magnesium grains. A large Mg grain can be seen in this micrograph, and its [1 $\bar{1}$ 0] zone axis SADP is presented. As shown in Fig. 5(d), the precipitates that have a rod-like morphology and an average grain size of 0.2 × 1.0 μm were identified as Mg_2Ni from electron diffraction [1 $\bar{1}$ 0] zone axis pattern. Thus, the microstructure consisted mainly of a considerable amount of microcrystalline Mg and Mg_2Ni and some $Mg_{12}Mm$ particles.

4. Discussion

By controlling the cooling rate of the melt-spun ribbon during solidification, various microstructures such as amorphous, nanocrystalline, and microcrystalline phases were obtained. Compared with the as-cast master alloy in Fig. 1, the grain size of melt-spun ribbon was remarkably reduced by rapid solidification, and mico- and nanosize grains were obtained. As shown in Figs. 2 and 3, a nearly single amorphous phase was obtained at a surface velocity of the copper wheel of 20.9 ms^{-1} except for minor nanocrystalline Mg and Mg_2Ni particles. By decreasing the surface velocity of the copper wheel from 10.5 to 3.1 ms^{-1}, the amount of crystalline phases increased significantly as shown in Figs. 4 and 5, that is the microstructure evolved from partially crystalline to fully crystalline. For example, the grain size increased from about 10 nm to 0.4 μm for crystalline Mg and from 4 × 10 nm to 0.2 × 1.0 μm for crystalline Mg_2Ni, respectively. The microstructure was fully crystalline when the surface velocity of the copper wheel was 3.1 ms^{-1}, a considerable amount of microcrystalline Mg and Mg_2Ni was formed, and some $Mg_{12}Ce$ particles were observed at the boundaries of Mg grains.

Previous work has demonstrated improved hydrogen storage properties of magnesium due to the formation of large amounts of amorphous phases and fine nanosize particles. Spassov et al. [18] and Spassov and Koster [19] studied hydrogen storage in rapidly solidified Mg-based Mg–Ni–RE (RE = Y or Mm) alloys. They reported that the difference in the hydrogenation properties between the as-quenched nano/amorphous and completely nanocrystalline (grain size in the range 100–150 nm) $Mg_{75}Ni_{20}Mm_5$ was insignificant. The best hydriding properties were obtained in the nanocrystalline/amorphous $Mg_{75}Ni_{20}Mm_5$ alloy with a maximum hydrogen capacity of 4.0 wt%. Huang

et al. [20,21] studied the nanocrystallization and hydrogenation properties of amorphous $Mg_{65}Cu_{25}Nd_{10}$ prepared by melt spinning. They reported that amorphous $Mg_{65}Cu_{25}Nd_{10}$ showed faster initial hydrogenation rate and higher hydrogen capacity (3.2 wt%) than partially crystalline and completely crystallized microstructural states.

The present melt-spun ribbon is expected to have increased hydrogen storage capacity and faster hydrogen exchange rates due to the increased amount of grain-boundary regions and amorphous regions. The higher hydrogen storage properties obtained by rapid solidification can be understood primarily from the modification of the morphological characteristics that determine the hydrogen diffusion paths. Orimo and Fujii [22] reported that hydrogen concentrated in three nanometer-scale regions: the grain interior region of Mg_2Ni, the grain-boundary region, and the amorphous region. The maximum hydrogen concentrations of the three regions were determined to be 0.3 wt% H in the grain interior region of Mg_2Ni, 4.0 wt% H in the grain boundary, and 2.2 wt% H in the amorphous region. It revealed that the hydrides were mainly formed in the grain-boundary and in the amorphous regions. In the present study, the ribbons that were melt-spun at highest solidification rate contain substantial amounts of amorphous phase and fine nanosize Mg_2Ni particles as shown in Figs. 3 and 4. Therefore, an optimal microstructure for hydrogen storage applications might have been produced.

5. Conclusions

The microstructural evolution of Mg-based Mg–20Ni–8Mm hydrogen storage alloy under various solidification rates were studied, and the following conclusions were drawn:

1. Microcrystalline, nanocrystalline, and amorphous microstructures were obtained by controlling the surface velocity of the copper wheel from 3.1, 10.5 to 20.9 ms^{-1}, respectively.
2. Compared with the as-cast master alloy, the grain size of the melt-spun ribbons was greatly refined. The microstructure containing a considerable amount of nanocrystalline Mg and Mg_2Ni in an amorphous matrix is expected to have the highest hydrogen storage capacity and the most rapid rate of hydrogen diffusion. Mischmetal-containing phases of $Mg_{12}Mm$ particles precipitated at the boundaries of magnesium grains, thus providing possible pathways for the enhanced hydrogen diffusion into the Mg.

Acknowledgment

The authors are grateful to the Norwegian Research Council for financial support.

References

[1] J. Bystrzycki, T. Czujko, R.A. Varin, J. Alloys Compd. 404 (2005) 507–510.
[2] Q. Li, K.C. Chou, K.D. Xu, Q. Lin, L.J. Jiang, F. Zhan, Intermetallics 14 (2006) 1386–1390.
[3] H.T. Yuan, Q.D. Li, H.N. Song, Y.J. Wang, J.W. Liu, J. Alloys Compd. 353 (2003) 322–326.
[4] F.C. Gennari, G. Urretavizcaya, J.J.A. Gamboa, G. Meyer, J. Alloys Compd. 354 (2003) 187–192.
[5] S.S.S. Raman, D.J. Davidson, J.L. Bobet, O.N. Srivastava, J. Alloys Compd. 333 (2002) 282–290.
[6] L.B. Wang, Y.J. Wang, H.T. Yuan, J. Mater. Sci. Technol. 17 (2001) 590–596.
[7] J.J. Jiang, M. Gasik, J. Power Sources 89 (2000) 117–124.
[8] D.J. Davidson, S.S.S. Raman, O.N. Srivastava, J. Alloys Compd. 292 (1999) 194–201.
[9] G. Liang, S. Boily, J. Huot, A. Van Neste, R. Schulz, Mater. Sci. Forum 269–272 (1998) 1049–1053.
[10] T. Spassov, U. Koster, J. Alloys Compd. 279 (1998) 279–286.
[11] T. Spassov, U. Koster, J. Alloys Compd. 287 (1999) 243–250.
[12] T. Spassov, L. Lyubenova, U. Koster, M.D. Baro, Mater. Sci. Eng. A 375–377 (2004) 794–799.
[13] K. Tanaka, Y. Kanda, M. Furuhashi, K. Saito, K. Kuroda, H. Saka, J. Alloys Compd. 295 (1999) 521–525.
[14] S.I. Yamamura, H.Y. Kim, H. Kimura, A. Inoue, Y. Arata, J. Alloys Compd. 339 (2002) 230–235.
[15] S. Yamaura, H. Kimura, A. Inoue, J. Alloys Compd. 358 (2003) 173–176.
[16] A. Zaluska, L. Zaluski, J.O. Ström-Olsen, J. Alloys Compd. 289 (1999) 197–206.
[17] S. Orimo, H. Fujii, K. Ikeda, Acta Mater. 45 (1997) 331–341.
[18] T. Spassov, V. Rangelova, N. Neykov, J. Alloys Compd. 334 (2002) 219–223.
[19] T. Spassov, U. Koster, Mater. Sci. Forum 307 (1999) 243–250.
[20] L.J. Huang, G.Y. Liang, Z.B. Sun, Y.F. Zhou, J. Alloys Compd., in press.
[21] L.J. Huang, G.Y. Liang, Z.B. Sun, J. Alloys Compd. 421 (2006) 279–282.
[22] S. Orimo, H. Fujii, Appl. Phys. A 72 (2001) 167–186.